The Astrophysical Journal, 680:119–129, 2008 June 10

SPITZER MID-INFRARED SPECTROSCOPY OF DISTANT X-RAY LUMINOUS ACTIVE GALACTIC NUCLEI

Kate Brand,[1] Dan W. Weedman,[2] Vandana Desai,[3] Emeric Le Floc'h,[4] Lee Armus,[5] Arjun Dey,[6] Jim R. Houck,[2] Buell T. Jannuzi,[6] Howard A. Smith,[7] and B. T. Soifer[3,5]

Received 2007 November 12; accepted 2008 January 29

ABSTRACT

We present mid-infrared spectroscopy of a sample of 16 optically faint infrared luminous galaxies obtained with the Infrared Spectrograph (IRS) on the *Spitzer Space Telescope*. These sources were jointly selected from *Spitzer* and *Chandra* imaging surveys in the NOAO Deep Wide-Field Survey Boötes field and were selected from their bright X-ray fluxes to host luminous AGNs. None of the spectra show significant emission from polycyclic aromatic hydrocarbons (PAHs; 6.2 μm equivalent widths <0.2 μm), consistent with their infrared emission being dominated by AGNs. Nine of the X-ray sources show 9.7 μm silicate absorption features. Their redshifts are in the range $0.9 < z < 2.6$, implying infrared luminosities of $\log L_{\rm IR} = 12.5$–$13.6\, L_{\odot}$. The average silicate absorption is not as strong as that of previously targeted optically faint infrared luminous galaxies with similar mid-infrared luminosities, implying that the X-ray selection favors sources behind a smaller column of Si-rich dust than non-X-ray selection. Seven of the X-ray sources have featureless power-law mid-infrared spectra. We argue that the featureless spectra likely result from the sources having weak or absent silicate and PAH features rather than the sources lying at higher redshifts, where these features are shifted out of the IRS spectral window. We investigate whether there are any correlations between X-ray and infrared properties and find that sources with silicate absorption features tend to have fainter X-ray fluxes and harder X-ray spectra, indicating a weak relation between the amount of silicate absorption and the column density of X-ray-absorbing gas.

Subject headings: galaxies: active — galaxies: starburst — infrared: galaxies — quasars: general

Online material: color figures

1. INTRODUCTION

Mid-infrared spectroscopy is a useful tool in investigating the extent to which starbursts and AGNs contribute to the luminosity of luminous infrared galaxies (LIRGs; Sanders et al. 1988). The infrared spectra of local LIRGs have been studied extensively with ISOPHOT, ISOCAM, and SWS on the *Infrared Space Telescope* (*ISO*; e.g., Lutz et al. 1998; Genzel et al. 1998; Rigopoulou et al. 1999; Tran et al. 2001) and more recently with the Infrared Spectrograph (IRS; Houck et al. 2004) on the *Spitzer Space Telescope* (Weedman et al. 2005; Brandl et al. 2006; Armus et al. 2007; Desai et al. 2007). The *Spitzer* IRS has also extended these studies to fainter sources at higher redshifts. A particularly interesting population of high-redshift optically faint infrared luminous sources (Yan et al. 2004; Brand et al. 2007; Fiore et al. 2008; Dey et al. 2008) has been discovered using the Multiband Imaging Photometer for *Spitzer* (MIPS; Rieke et al. 2004). Various observing programs with the *Spitzer* IRS have found that MIPS sources at flux density levels of $f_{\nu}(24\ \mu{\rm m}) \geq 0.8$ mJy with optical magnitudes $R \gtrsim 24$ are typically at $z \sim 2$–3 (Houck et al. 2005; Weedman et al. 2006b; Yan et al. 2007; Sajina et al. 2007). The infrared spectra exhibit a wide range of properties, from deep 9.7 μm silicate absorption features and/or strong polycyclic aromatic hydrocarbon (PAH) emission features to featureless power-law continua. This obscured population is important in determining how much light originates from starbursts and AGNs at epochs in the universe when their luminosity density was at its maximum. Given that their optical faintness makes optical follow-up difficult, understanding how to characterize these sources using their infrared spectra is important in understanding their energetics.

One approach in understanding the contribution of starbursts and AGNs to the infrared emission of optically faint infrared sources is to investigate the infrared spectra of sources also selected in other wave bands. For example, at one extreme we can study sources selected on the basis of large far-infrared flux densities, which we might expect to contain cool dust and show signatures of starbursts. In Brand et al. (2008) we presented the IRS spectra of 11 70 μm–selected optically faint infrared luminous galaxies and found that seven had large 6.2 μm PAH equivalent widths, consistent with them being powerful starburst galaxies. Four of the galaxies showed deep silicate absorption features, and their properties suggested that AGNs are likely to be the dominant origin of their large mid-infrared luminosities.

At the other extreme, we can consider sources selected on the basis of X-ray flux, which we might expect to show spectral signatures of AGNs. Weedman et al. (2006a) presented IRS spectra of nine X-ray loud optically faint infrared luminous galaxies selected from the *Spitzer* Wide-Area Infrared Extragalactic survey (SWIRE; Lonsdale et al. 2004). Eight sources have silicate absorption features, and one source has a featureless power-law mid-infrared spectrum.

In this paper we present *Spitzer* IRS spectra of 16 optically faint infrared galaxies in the Boötes field of the NOAO Deep

[1] Space Telescope Science Institute, 3700 San Martin Drive, Baltimore, MD 21218; brand@stsci.edu.
[2] Astronomy Department, Cornell University, Ithaca, NY 14853.
[3] Division of Physics, Mathematics and Astronomy, California Institute of Technology, 320-47, Pasadena, CA 91125.
[4] Institute for Astronomy, University of Hawaii, 2680 Woodlawn Drive, Honolulu, HI 96822.
[5] *Spitzer* Science Center, California Institute of Technology, 220-6, Pasadena, CA 91125.
[6] National Optical Astronomy Observatory, 950 North Cherry Avenue, Tucson, AZ 85726.
[7] Harvard-Smithsonian Center for Astrophysics, 60 Garden Street, Cambridge, MA 02138.

TABLE 1
Optical and Infrared Properties

IRS ID	MIPS Name	B_W[a,b] (mag)	R[a,b] (mag)	I[a,b] (mag)	K[a,b] (mag)	$f_\nu(3.6)$[c] (mJy)	$f_\nu(4.5)$[c] (mJy)	$f_\nu(5.8)$[c] (mJy)	$f_\nu(8)$[c] (mJy)	$f_\nu(24)$[c] (mJy)	$f_\nu(70)$ (mJy)	$f_\nu(160)$ (mJy)	$R-[24]$ (mag)
Bootes X1	SST24 J143048.3+322532	24.00	23.11	22.33	...	0.13	0.22	0.77	0.68	3.15	<12	<120	14.70
Bootes X2	SST24 J142731.3+324434	25.54	23.04	21.51	...	0.09	0.12	0.20	0.59	2.61	<15	<100	14.42
Bootes X3	SST24 J142609.0+333303	23.33	22.80	21.84	18.29[d]	0.05	0.06	0.10	0.18	2.49	<20	<120	14.13
Bootes X4	SST24 J143234.9+333637	24.53	22.96	21.53	18.65[d]	0.18	0.35	0.73	1.68	2.92	30 ± 6	110 ± 22	14.47
Bootes X5	SST24 J142625.5+334051	25.14	23.53	22.04	18.00[d]	0.21	0.32	0.52	0.82	2.11	...	<120	14.69
Bootes X6	SST24 J143232.6+335903	23.09	22.79	22.10	17.85[d]	0.04	0.05	0.16	0.38	2.42	10 ± 2	80 ± 16	14.09
Bootes X7	SST24 J143038.4+340929	24.34	22.86	21.67	18.53[d]	0.06	0.10	0.17	0.35	2.40	12 ± 2	<100	14.15
Bootes X8	SST24 J143301.5+342341	23.48	22.85	22.54	18.32[d]	0.10	0.16	0.35	0.62	2.17	<15	<120	14.04
Bootes X9	SST24 J142849.0+343432	23.58	22.35	21.14	18.11[e]	0.08	0.10	0.13	0.33	2.36	<15	<100	13.60
Bootes X10	SST24 J143834.9+343839	22.76	22.44	22.58	...	0.06	−1.0[g]	0.25	−1.0[g]	2.25	<20	<150	13.66
Bootes X11	SST24 J143715.1+345323	24.15	23.73	23.06	...	0.16	0.27	0.49	0.95	2.51	<15	<120	15.07
Bootes X12	SST24 J142537.8+351735	24.21	22.12	20.69	18.30[e]	0.09	0.12	0.21	0.38	2.28	25 ± 5	<120	13.36
Houck 13.....	SST24 J143644.2+350627	24.71	23.69	23.36	19.11[f]	0.04	0.10	0.32	0.69	2.34	9.1 ± 2.5[f]	43 ± 12[h]	14.96
X-Ray Bright Subsample													
Bootes X13	SST24 J143723.4+334308	24.96	22.78	22.49	...	0.03	0.03	0.04	0.11	1.44	20 ± 4	<120	13.52
Bootes X14	SST24 J142707.0+325213	...	22.03	...	...	0.19	0.16	0.19	0.25	1.22	<12	<100	12.59
Bootes X15	SST24 J143359.0+331301	23.95	22.40	21.06	17.15[d]	0.23	0.29	0.42	0.61	1.92	<15	<120	13.45

[a] All quoted magnitudes are Vega magnitudes from the NDWFS DR3 (B. T. Jannuzi et al., in preparation).
[b] Errors on B_W-, R-, I-, and K-band magnitudes are <0.1.
[c] Errors on $f_\nu(3.6)$, $f_\nu(4.5)$, $f_\nu(5.8)$, $f_\nu(8)$, and $f_\nu(24)$ flux densities are <0.1 mJy.
[d] K_s-band magnitudes from the FLAMEX survey (Elston et al. 2006).
[e] K-band magnitudes from the NDWFS (A. Dey et al., in preparation).
[f] K-band magnitudes from Keck NIRC observations.
[g] Because Bootes X10 lies at the edge of our IRAC coverage, no detections were found in this band.
[h] Value from deeper imaging data presented in K. Tyler et al. (in preparation).

Wide-Field Survey (NDWFS; Jannuzi & Dey 1999) which are selected to be X-ray loud. This significantly increases the number of X-ray loud optically faint infrared luminous galaxies thus far studied and extends the sample to higher X-ray and 24 μm luminosities. A cosmology of $H_0 = 70\ \mathrm{km\ s^{-1}\ Mpc^{-1}}$, $\Omega_M = 0.3$, and $\Omega_\Lambda = 0.7$ is assumed throughout.

2. SOURCE SELECTION

Our sample is selected from the Boötes field of the NDWFS (Jannuzi & Dey 1999). The combination of the large survey area (8.2 deg^2 with overlapping MIPS and optical coverage) and existing *Spitzer* MIPS, IRAC, *Chandra*, and deep optical imaging data makes this an ideal data set for multiwavelength comparisons of sources. The MIPS data were obtained with an effective integration time at 24 μm of $\sim$90 s per sky pixel, reaching a 5 σ detection limit of $\sim$0.3 mJy for unresolved sources. The resulting source lists contain $\approx$28,000 sources with $f_\nu(24\ \mu\mathrm{m}) > 0.3$ mJy. The XBoötes survey was undertaken using ACIS-I on the *Chandra X-ray Observatory* with 5 ks exposures over the entire Boötes field (Murray et al. 2005; Kenter et al. 2005; Brand et al. 2006a). It comprises 3293 point sources with four or more X-ray counts, corresponding to a limiting flux of $f_{0.5\text{–}7\ \mathrm{keV}} = 8.1 \times 10^{-15}\ \mathrm{ergs\ cm^{-2}\ s^{-1}}$. An 8.5 deg^2 region of the Boötes field has been mapped in all four *Spitzer* IRAC bands by the IRAC Shallow Survey (Eisenhardt et al. 2004), reaching 5 σ limits of 6.4, 8.8, 51, and 50 μJy at 3.6, 4.5, 5.8, and 8 μm, respectively.

Using the XBoötes and MIPS 24 μm catalogs, we selected a sample of 16 X-ray loud sources in the Boötes field for *Spitzer* IRS observations. We selected all 13 of the sources with >4 X-ray counts ($f_{0.5\text{–}7\ \mathrm{keV}} > 8.1 \times 10^{-15}$ ergs cm^{-2} s^{-1}), $f_\nu(24\ \mu\mathrm{m}) > 2$ mJy, and $R > 22$ mag (the "main" sample). We supplemented this sample with three extra sources (Bootes X13, X14, and X15) which were slightly fainter at 24 μm [$f_\nu(24\ \mu\mathrm{m}) > 1$ mJy] but were particularly powerful X-ray sources (hereafter denoted as the "X-ray bright" subsample with 48, 34, and 19 X-ray counts corresponding to $f_{0.5\text{–}7\ \mathrm{keV}} = 9.2$, 6.5, and 3.7×10^{-14} ergs cm^{-2} s^{-1}, respectively). Because of their different selection criteria, we identified the X-ray bright subsample separately throughout the analysis and considered the conclusions with and without their inclusion.

The basic optical and infrared properties of the sample are shown in Table 1. Ten out of 16 of the sources have fairly red optical-to-infrared colors and qualify as dust-obscured galaxies based on the criterion ($R - [24] > 14$) presented in Dey et al. (2008). None of the members of our sample have redshifts from optical spectroscopy. The X-ray properties are presented in Table 2. At $z > 1$, the X-ray luminosities are far larger than can be attributed to a starburst and must be attributed to an AGN. At $z = 0.9$ (the lowest measured source redshift; see below), the minimum X-ray flux, $f_{0.5\text{–}7\ \mathrm{keV}} = 8.1 \times 10^{-15}$ ergs cm^{-2} s^{-1}, corresponds to an X-ray luminosity of $\approx 3 \times 10^{43}$ ergs s^{-1}. If this was all due to star formation, it would imply an unfeasibly large star formation rate (SFR) of $\approx$5000 $M_\odot\ \mathrm{yr^{-1}}$ (Grimm et al. 2003).

3. OBSERVATIONS AND DATA ANALYSIS

The spectroscopic observations were made with the IRS Short Low module in order 1 only (SL1) and with the Long Low module in orders 1 and 2 (LL1 and LL2), described in Houck et al. (2004). These orders give low-resolution spectral coverage from $\sim$8 to $\sim$35 μm. The integration times for individual sources are given in Table 3. Data were processed with version 13.0 of the SSC pipeline, and extraction of the source spectra was done with the

TABLE 2
X-RAY PROPERTIES

IRS ID	X-Ray Name	X-Ray Counts[a]	Hardness Ratio[b]	f_X[c]	$\log_{10}(f_X/f_{opt})$[d]	$\log(L_X)$[e] (ergs s^{-1})
Bootes X1	CXOXB J143048.3+322531	5 ± 2.2	$1.00^{+0.00}_{-0.48}$	8.5 ± 5.6	0.67	44.22
Bootes X2	CXOXB J142731.4+324435	6 ± 2.4	$0.68^{+0.19}_{-0.25}$	10.6 ± 5.9	0.74	43.63
Bootes X3	CXOXB J142609.0+333304	5 ± 2.2	$0.20^{+0.26}_{-0.28}$	9.5 ± 5.9	0.60	44.44
Bootes X4	CXOXB J143234.9+333636	4 ± 2.0	$0.51^{+0.29}_{-0.37}$	8.1 ± 5.6	0.59	43.75
Bootes X5	CXOXB J142625.5+334052	7 ± 2.6	$-0.16^{+0.20}_{-0.19}$	14.3 ± 6.7	1.07	44.23
Bootes X6	CXOXB J143232.6+335902	21 ± 4.6	$-0.44^{+0.07}_{-0.06}$	43.8 ± 10.0	1.26	44.25
Bootes X7	CXOXB J143038.5+340928	7 ± 2.6	$0.72^{+0.16}_{-0.22}$	14.0 ± 6.7	0.79	43.97
Bootes X8	CXOXB J143301.5+342343	14 ± 3.7	0.00 ± 0.10	27.1 ± 8.4	1.07	44.95
Bootes X9	CXOXB J142849.0+343432	6 ± 2.4	$0.67^{+0.19}_{-0.25}$	12.5 ± 6.5	0.54	...
Bootes X10	CXOXB J143835.0+343839	9 ± 3.0	0.11 ± 0.15	18.0 ± 7.3	0.73	44.99
Bootes X11	CXOXB J143715.1+345323	5 ± 2.2	$-0.20^{+0.27}_{-0.26}$	20.5 ± 6.0	1.30	...
Bootes X12	CXOXB J142537.8+351735	29 ± 5.4	-0.10 ± 0.05	56.8 ± 11.1	1.10	...
Houck 13	CXOXB J143644.2+350626	7 ± 2.6	$0.43^{+0.18}_{-0.20}$	13.2 ± 6.5	1.10	44.55
X-Ray Bright Subsample						
Bootes X13	CXOXB J143723.5+334307	48 ± 6.9	-0.21 ± 0.03	92.0 ± 13.9	1.58	...
Bootes X14	CXOXB J142707.0+325212	34 ± 5.8	-0.47 ± 0.04	64.9 ± 12.1	1.21	...
Bootes X15	CXOXB J143359.1+331300	19 ± 4.3	0.47 ± 0.07	37.2 ± 9.6	1.03	...

[a] Counts in observed total (0.5–7 keV) band and their associated Poisson errors.
[b] The hardness ratio is defined as H−S/H+S, where H denotes the X-ray counts in the hard (2–7 keV) band and S denotes the X-ray counts in the soft (0.5–2 keV) band.
[c] Observed 0.5–7 keV X-ray flux and error in 10^{-15} ergs cm^{-2} s^{-1} assuming a power-law spectrum with photon index $\Gamma = 1.7$ and a galactic column density of 1×10^{20} cm^2 (Stark et al. 1992). No correction has been made for intrinsic X-ray absorption.
[d] X-ray-to-optical (R-band) flux ratio defined as $\log_{10}(f_X/f_{opt}) = \log_{10}(f_X) + 0.4R + 5.5$ (Brand et al. 2006a).
[e] Rest-frame 0.5–7 keV X-ray luminosity calculated using redshifts in Table 3.

SMART analysis package (Higdon et al. 2004). For details of the observational and data analysis techniques, we refer the reader to Brand et al. (2008).

4. RESULTS

The IRS spectra of all 16 X-ray-selected sources are shown in Figure 1. Although the IRS spectrum of Houck 13 was presented in Houck et al. (2005), it satisfies the selection criteria of the main sample, and we include it again here for completeness. Nine out of 13 members of the main sample (and 9 out of 16 members of the total "main + X-ray bright" sample) exhibit identifiable 9.7 μm silicate absorption features ($S_{10} < -0.4$;[8] hereafter described as "absorption-dominated" sources and denoted by "abs" in Table 3). A further 4 out of 13 members of the main sample (and 7 out of 16 members of the total "main + X-ray bright" sample) exhibit power-law spectra with no convincing features (hereafter described as "power-law" sources and denoted by "pow" in Table 3); either they have only weak silicate absorption features or they are at $z > 2.6$ and the absorption feature does not fall within the observable IRS bandwidth. Bootes X6 may have a weak silicate emission feature if it is at $z = 0.9$. Given that this is highly uncertain without other convincing features in the spectrum, we classify Bootes X6 as a power-law source. None of the sources show convincing PAH emission features, although, given their uncertain or unknown redshifts, there may be weak PAH emission in some individual sources. We discuss each class in turn.

4.1. *Absorption-Dominated Sources*

For the absorption-dominated sources, redshifts are determined primarily from the localized maximum in the IRS continuum, or "hump," which is blueward of the absorption feature. This feature is produced by absorption on either side of the feature and with a possible contribution of 7.7 μm PAH emission in composite sources. We determine redshifts by assuming this hump has a rest-frame wavelength of 7.9 μm (see the average spectra in Hao et al. 2007 and Spoon et al. 2007). Comparison of IRS redshifts with optical redshifts for similar absorbed sources (e.g., Brand et al. 2007; Dey et al. 2008) suggests that they can be uncertain to ± 0.2 in z.

For the absorption-dominated sources, the overall nature of the infrared spectra can be best considered by assembling the average IRS spectrum. This allows consistent features within individual spectra to be seen with improved signal-to-noise ratios. This is achieved by wavelength-correcting each individual unsmoothed spectrum to the rest frame ($z = 0$), interpolating them to a common wavelength scale of ~ 0.1 μm $pixel^{-1}$, and taking a straight (nonweighted) average at each wavelength position. The averaged spectrum is shown in Figure 2 (*top*). The most dominant feature is the silicate absorption feature at 9.7 μm. The average silicate absorption strength (as defined in Table 3) is $S_{10} = -1.0$ (with individual values ranging from -0.4 to -2.9). For comparison, we also show the average spectrum of the absorption-dominated 70 μm–selected sources presented in Brand et al. (2008; Fig. 2, *bottom*). Even though the X-ray-selected absorption-dominated sources have an average $R - [24]$ color similar to that of the 70 μm–selected absorption-dominated sources, they have a much shallower average silicate absorption ($S_{10} = -1.0$ compared to $S_{10} = -2.1$). The average silicate absorption of the X-ray sample is substantially less than the median value for local ULIRGs (Hao et al. 2007; Spoon et al. 2007) and the optically obscured sample observed by Houck et al. (2005) and Weedman et al. (2006b) and is slightly larger that the median value for Seyfert 2 AGNs (-0.6; Hao et al. 2007).

The individual spectra show no evidence for PAH emission (6.2 μm equivalent width <0.2 μm; see Table 3), although there

[8] S_{10} is defined in Table 3.

TABLE 3

IRS and Derived Physical Properties

IRS ID	Exp. Time SL[a] (s)	Exp. Time LL[b] (s)	IRS z	νL_ν(6 μm) log ($L_\odot$)	νL_ν(8 μm) log ($L_\odot$)	L_{IR}[c] log ($L_\odot$)	$f_\nu(15)/f_\nu(6)$	S_{10}[d]	PAH EW[e] (μm)	SFR[f] ($M_\odot$ yr^{-1})	L_{IR}(SFR)[g] log ($L_\odot$)	IRS Class[h]
Bootes X1	240	480	1.7	12.2	12.6	13.3	...	−0.4	<0.05	<1380	<12.8	abs
Bootes X2	360	720	0.9	11.5	11.8	12.5	3.3	−1.0	<0.04	<190	<12.0	abs
Bootes X3	480	960	2.0[i]	12.2	12.6	13.3	...	−0.4	<0.20	<1170	<12.9	abs
Bootes X4	360	720	1.12	12.2	12.4	13.1	2.4	−1.4	<0.04	<450	<12.4	abs
Bootes X5	480	960	1.4	12.0	12.3	13.0	2.8	−0.4	<0.09	<590	<12.5	abs
Bootes X6	360	720	0.9	...	...	...	...	...	...	...	...	pow/em?
Bootes X7	480	960	1.1	11.5	11.9	12.6	6.3	−0.5	<0.05	<110	<11.7	abs
Bootes X8	480	960	2.1	12.3	12.5	13.2	...	−0.6	<0.05	<560	<12.5	abs
Bootes X9	480	960	...	...	...	...	...	...	...	...	...	pow
Bootes X10	480	960	2.6	12.6	12.9	13.6	...	<−1.8	<0.10	<1670	<12.9	abs
Bootes X11	480	960	...	...	...	...	...	...	...	...	...	pow
Bootes X12	480	960	...	...	...	...	...	...	...	...	...	pow
Houck 13.....	480	720	1.95	12.3	12.5	13.2	...	−2.9	<0.03	<420	<12.3	abs
X-Ray Bright Subsample												
Bootes X13	480	1200	...	...	...	...	...	...	...	...	...	pow
Bootes X14	480	1200	...	...	...	...	...	...	...	...	...	pow
Bootes X15	480	1200	...	...	...	...	...	...	...	...	...	pow

[a] Total integration times in SL1.

[b] Total integration times in each of LL1 and LL2.

[c] The total infrared luminosity, $L_{IR} = L(8–1000\ \mu m)$, as estimated from the measured rest-frame 8 μm flux density using the relation for the template of Mrk 231 [$L_{IR} = 5.0\nu L_\nu(8\ \mu m)$].

[d] Silicate absorption strength is defined as $S_{10} = \ln[f_{obs}(10\ \mu m)/f_{cont}(10\ \mu m)]$, where $f_{obs}(10\ \mu m)$ is the observed flux density at the peak of the 10 μm feature and $f_{cont}(10\ \mu m)$ is the continuum flux at the peak wavelength, extrapolated from the continuum to either side.

[e] Rest-frame equivalent width of a 6.2 μm PAH emission feature.

[f] Maximum SFR estimated from the measured limit on the 6.2 μm PAH emission feature using the relation of Pope et al. (2008).

[g] Maximum infrared luminosity associated with star formation estimated from the measured limit on the 6.2 μm PAH emission feature using the relation of Pope et al. (2008).

[h] Absorption-dominated and featureless power-law sources are denoted "abs" and "pow," respectively; "em?" denotes possible silicate emission.

[i] The redshift could be $z = 1.5$ if instead of silicate absorption at an observed wavelength of 29 Å, the spectrum is interpreted as having silicate emission at an observed wavelength of ≈24 Å. However, silicate emission is generally only observed in type I AGNs, which tend to have much brighter optical magnitudes for such bright 24 μm emission (e.g., Brown et al. 2006).

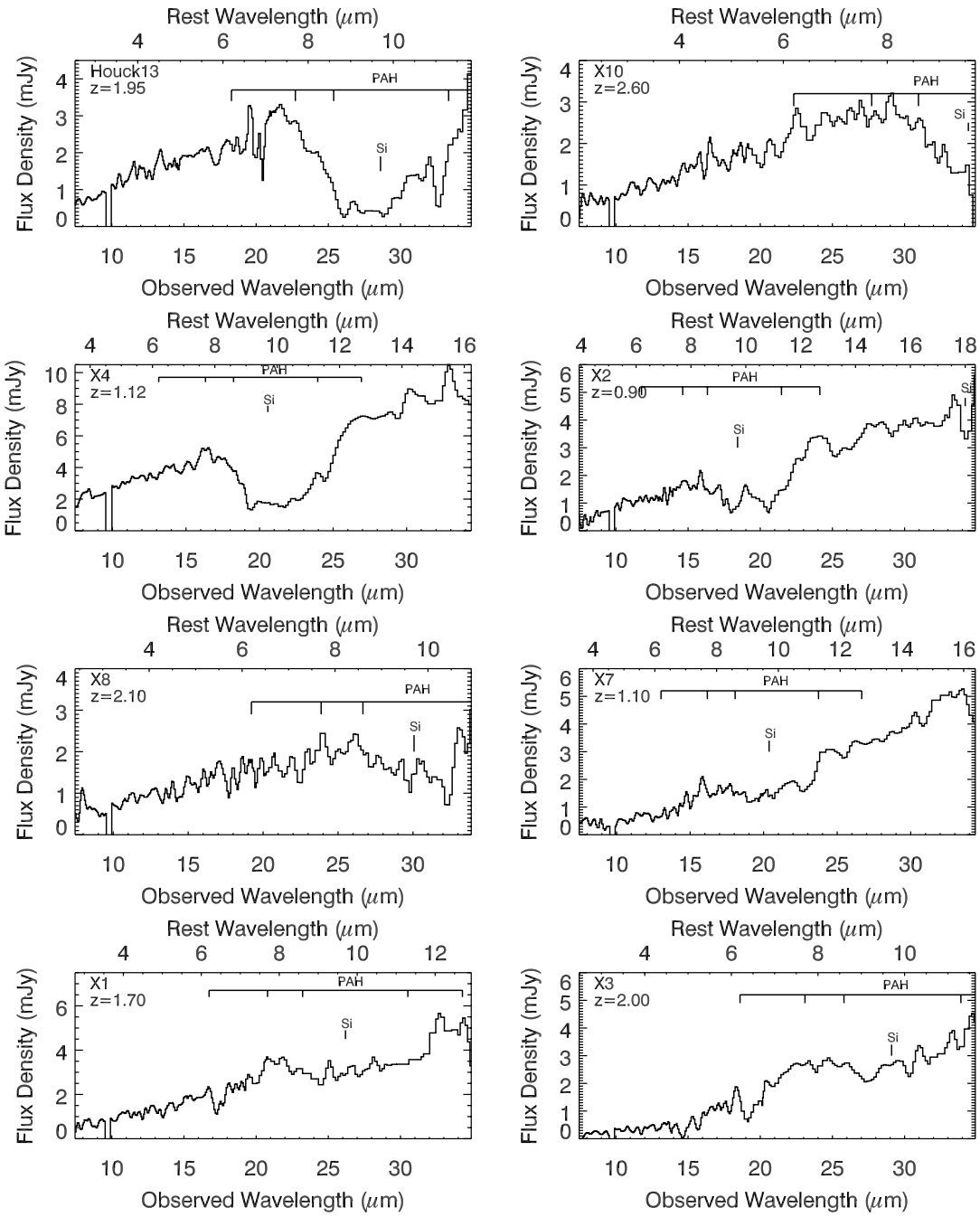

FIG. 1.—IRS spectra of X-ray-selected optically faint infrared luminous galaxies ordered by their silicate absorption strengths. The IRS spectrum of Houck 13 was published in Houck et al. (2005). The spectra are boxcar-smoothed over a resolution element (approximately 2 pixels). In cases where we have an estimated redshift, the expected positions of the PAH emission features and silicate absorption features are shown. A typical noise spectrum of IRS observations with similar 24 μm flux densities and exposure times can be found in Brand et al. (2008).

is a hint of the 6.2 and 7.7 μm PAH features in the average spectrum. However, because of the redshift uncertainties for the individual spectra, it is difficult to be confident in any weak, narrow emission-line features that appear in the average. The possible feature at 7.7 μm could also be due to the [Ne VI] emission line at 7.6 μm. For each individual source, we use the noise spectrum to estimate the maximum flux from the 6.2 μm PAH emission feature (we estimate the flux of the nearest noise feature to 6.2 μm). We then use the relation of Pope et al. (2008) to estimate the corresponding maximum SFR and infrared luminosity associated with star formation. The values are shown in Table 3. In some cases, the spectra are not sensitive enough to put a useful limit on the SFR. Bootes X2 and Bootes X7 have the lowest limits of SFR < 190 and $<100\ M_{\odot}\ \mathrm{yr}^{-1}$, respectively, corresponding to infrared luminosities associated with star formation of $\log L_{\mathrm{IR}} < 12.0$ and <11.7, respectively. Comparing these values to the total infrared luminosity estimated from the rest-frame 8 μm flux density suggests that less than 30% and 13% of the total infrared luminosities are from star formation processes.

Weak indications are present in the average for [Ne II], [Ne V], and [Ne III] emission lines. The relative intensities of these lines are $\sim 0.7 : 1 : 1$. The presence of [Ne V] is a strong AGN indicator (Lutz et al. 1998; Farrah et al. 2007). The relative intensities show that the [Ne V] is stronger than that of local Seyferts such as

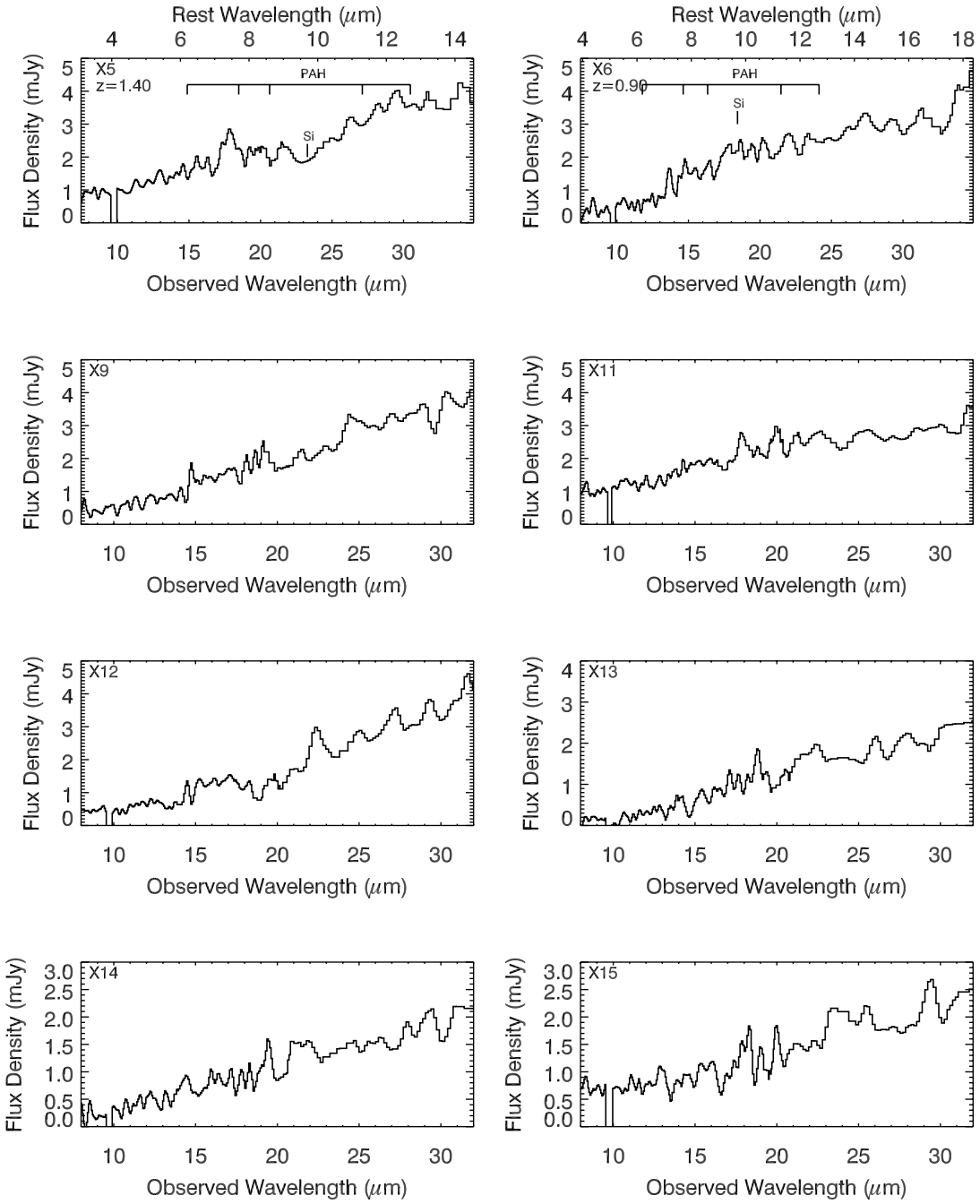

FIG. 1—*Continued*

NGC 4151, Mrk 3, and Cen A (Weedman et al. 2005). If there is a contribution of 12.7 μm PAH emission to the [Ne II] line in the stacked spectrum, it makes this effect even larger. This may indicate a higher ionization of the narrow-line region by the more powerful AGNs in these sources.

We have measured the luminosities at 5.8 μm to determine the continuum luminosity just shortward of the 6.2 μm PAH feature and at a wavelength without strong absorption (e.g., Brandl et al. 2006; Sajina et al. 2007; Hao et al. 2007; see Table 3 for individual values). The absorption-dominated sources have a median luminosity of $\nu L_\nu(6\ \mu\mathrm{m}) = 6 \times 10^{45}$ ergs s^{-1} ($1.5 \times 10^{12}\ L_\odot$). These are very luminous sources, exceeding most local AGNs in the sample of Hao et al. (2007): Seyfert 2 galaxies in that sample have median $\nu L_\nu(6\ \mu\mathrm{m}) \sim 10^{10}\ L_\odot$, and ULIRGs have $\nu L_\nu(6\ \mu\mathrm{m}) \sim 10^{11}\ L_\odot$. Desai et al. (2007) find that local ULIRGs span the range $\nu L_\nu(6\ \mu\mathrm{m}) = 1 \times 10^{10}$–$5 \times 10^{12}\ L_\odot$. Our sources lie at the upper end of this range. The most luminous X-ray source, at $\nu L_\nu(6\ \mu\mathrm{m}) = 4 \times 10^{12}\ L_\odot$, is nearly as luminous as the most luminous source yet published from IRS spectra, source 9 in Houck et al. (2005), with $\nu L_\nu(6\ \mu\mathrm{m}) = 5.9 \times 10^{12}\ L_\odot$.

We estimate the total infrared luminosity, $L_{\mathrm{IR}} = L(8$–$1000\ \mu\mathrm{m})$, of each of the absorption-dominated sources. The conversion factors vary significantly depending on the template adopted for the conversion (Caputi et al. 2007). Because we expect the infrared emission to be dominated by obscured AGN activity, we use the conversion for the template Mrk 231, $L_{\mathrm{IR}} = 5\nu L_\nu(8\ \mu\mathrm{m})$, where the rest-frame 8 μm flux density is measured directly from the IRS spectra. The estimates are about a factor of 7 lower than

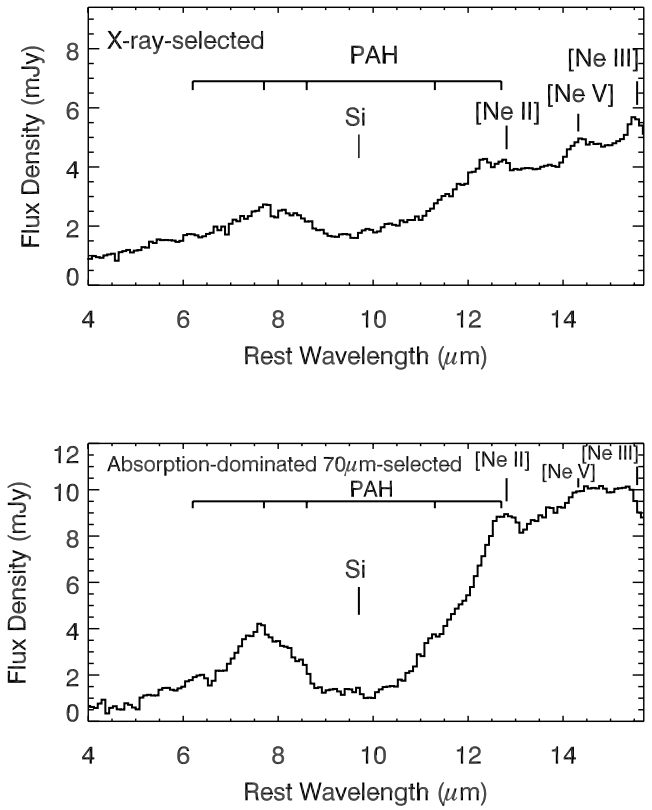

FIG. 2.—Average IRS spectrum of X-ray sources with redshifts (*top*). For comparison, the average IRS spectra of absorption-dominated 70 μm sources from Brand et al. (2008) is also shown (*bottom*). The expected positions of typically strong emission lines and the silicate absorption line are shown. The average spectrum combines the individual unsmoothed rest-frame spectra and is not smoothed.

one would obtain using templates of starburst-dominated galaxies such as Arp 220, and this explains our smaller $L_{\rm IR}$ compared to that of Houck et al. (2005) for Houck 13, which was estimated from F00183-7111. The infrared luminosities confirm that the absorption-dominated sources are all ultraluminous ($L_{\rm IR} > 10^{12}\ L_{\odot}$) or hyperluminous ($L_{\rm IR} > 10^{13}\ L_{\odot}$) infrared galaxies.

4.2. *Power-Law Sources*

Given the lack of features and/or optical follow-up of the power-law sources, we do not have redshifts for these sources. We therefore cannot construct an average spectrum or determine luminosities. The spectra of the power-law sources must have weak or absent silicate features (6.2 μm PAH equivalent widths $\lesssim$0.2 μm), or they lie beyond $z \sim 2.6$, causing their absorption features to fall longward of the IRS wavelength limit. It is difficult to determine whether silicate emission exists in these sources, given our lack of redshift information and that the silicate emission feature is generally weaker than the absorption feature. However, Bootes X6 may have a weak silicate emission feature if it is at $z = 0.9$. All three members of the "X-ray bright" subsample are power-law sources.

5. DISCUSSION

5.1. *IRS Spectra*

All the X-ray-selected sources have infrared spectra consistent with their mid-infrared luminosities being dominated by emission originating from AGN activity. This is expected given that their high X-ray luminosities imply that they host luminous AGNs, which should dominate their infrared spectra. We find a larger fraction of power-law sources (4 out of 13 of the main sample and 7 out of 16 of the total [main + X-ray bright] sample) than is found in the SWIRE sample of Weedman et al. (2006a; they find only 1 out of 9 to have a featureless power-law spectrum in their sample, which has an X-ray limit $\approx$8 times fainter than that of our sample). This may in part be due to them having accurate optical redshifts, which make it easier to identify features. It could also be due to our selection of more luminous X-ray sources, which are less likely to be heavily obscured and exhibit silicate absorption. This hypothesis is supported by the fact that 6 out of 7 of the power-law sources are also the brightest X-ray sources in the sample.

To explain the lack of a silicate absorption feature in their IRS spectra, the power-law sources must have weak or absent silicate features or they must lie beyond $z \sim 2.6$. We argue that the latter is unlikely given that they are among the brightest X-ray sources in our sample. If at $z > 2.6$, they must be extremely intrinsically luminous. Assuming a canonical power-law spectrum with photon index $\Gamma = 1.7$, the typical X-ray flux of $f_{0.5\text{–}7\ \rm keV} = 4 \times 10^{-14}$ ergs cm^{-2} s^{-1} corresponds to a rest-frame X-ray luminosity of $L_{0.5\text{–}7\ \rm keV} = 2 \times 10^{45}$ ergs s^{-1} at $z = 2.6$, which would suggest that they were among the most powerful quasars known. If at $z > 2.6$, these sources would be significantly more X-ray luminous than any of the sources at $z < 2.6$. We would not expect a sharp difference in the luminosities of sources at higher redshifts. Furthermore, only 0.7% of the $\sim$1000 X-ray sources in the *Chandra* XBoötes survey (Kenter et al. 2005) with spectroscopic redshifts from AGES (C. Kochanek et al., in preparation) have luminosities this high. In the following discussion, we assume that these sources are at similar redshifts to the rest of the X-ray-selected sources and that they must have weak or absent silicate features.

5.2. *Infrared Colors of X-Ray-Selected AGNs*

In Figure 3 we show the IRAC color-color diagram for our IRS sources. To increase the number of X-ray-selected sources, we also plot the nine X-ray-selected IRS sources from the Lockman Hole field of the SWIRE survey presented by Weedman et al. (2006a). The SWIRE sample is selected to have $f_\nu(24\ \mu{\rm m}) > 0.9$ mJy, $f_{0.3\text{–}8\ \rm keV} > 10^{-15}$ ergs cm^{-2} s^{-1}, and $R > 22$ mag. The X-ray flux limit still corresponds to typical AGN luminosities at these redshifts. To determine the location in color-color space of these sources in comparison to the general 24 μm population, we also plot the distribution of the $\approx$10,000 MIPS Boötes sources with $f_\nu(24\ \mu{\rm m}) > 0.5$ mJy. The rough regions expected to be inhabited by different populations are shown. We also plot the empirical line of Stern et al. (2005; see also Lacy et al. 2004) to separate AGN-dominated sources from Galactic stars and normal galaxies.

Twenty out of 25 of the X-ray-selected sources lie within the AGN region of Stern et al. (2005). Hickox et al. (2007) show that large amounts of extinction ($A_v > 50$) toward the active nucleus and/or a large contribution from a starburst can cause the IRAC colors of an object to fall outside of the Stern et al. (2005) region. Because our sources are largely within the AGN region, they are unlikely to be heavily extincted or have a large starburst contribution to their mid-infrared emission. There appears to be no correlation between the position in IRAC color-color space with the presence of the silicate absorption strength, again supporting the hypothesis that the silicate feature arises in the cooler gas which is traced by longer infrared wavelengths. The sources in the X-ray bright subsample appear to have slightly bluer colors, which may demonstrate that they are less dust-obscured. The

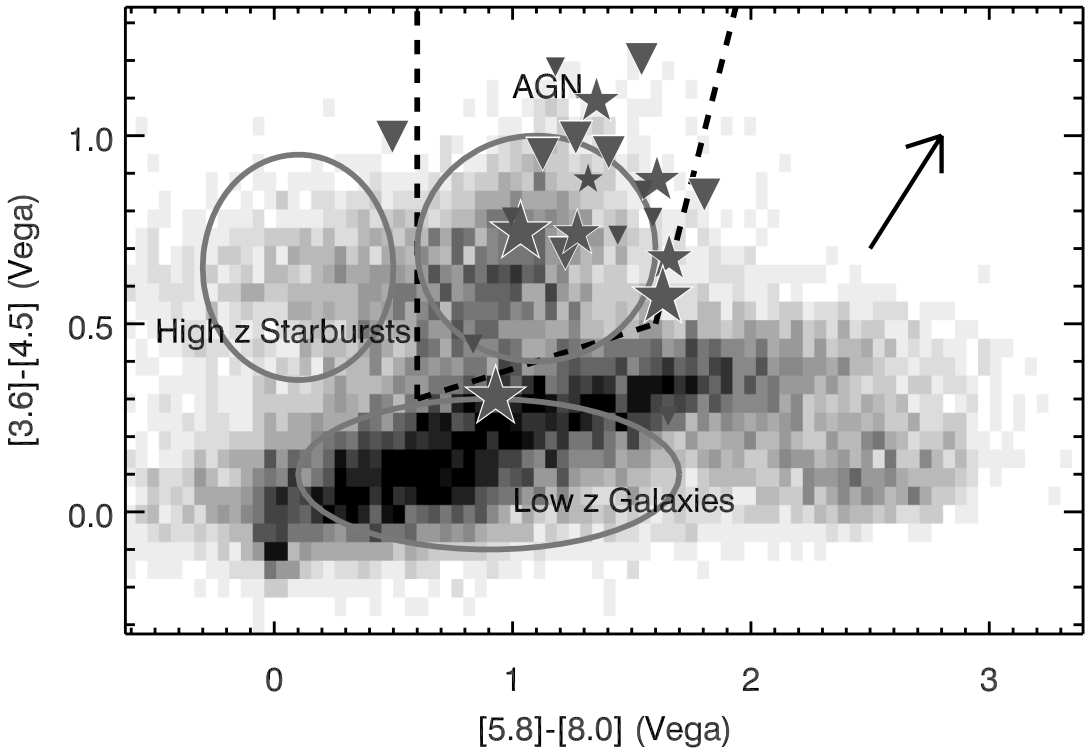

FIG. 3.— IRAC color-color diagram for X-ray-selected IRS sources (*large symbols*). The Boötes X-ray-selected sources are denoted by large symbols (with the largest symbols denoting the X-ray bright subsample). The fainter X-ray sources from Weedman et al. (2006a) are also shown (*small symbols*). The sources are split into silicate absorption-dominated sources (*triangles*) and power-law-dominated sources (*stars*). We show the distribution of all ≈10,000 MIPS sources with $f_\nu(24\ \mu\mathrm{m}) > 0.5$ mJy in gray scale. The rough regions expected to be inhabited by different populations are also shown. The dashed line is that proposed by Stern et al. (2005) to empirically separate AGNs from Galactic stars and normal galaxies. The arrow represents the reddening vector, estimated using the extinction curve of Draine (2003) for a source at $z = 1$ reddened by a dust column corresponding to $R_v = 3.1$. [*See the electronic edition of the Journal for a color version of this figure.*]

IRAC color-color classification is expected to deteriorate at $z \gtrsim 1$ as the observed IRAC bands are pushed toward lower wavelengths in which the stellar light dominates over hot dust emission (Stern et al. 2005; Lacy et al. 2004). However, it likely holds to higher redshifts for the most luminous sources because the near-infrared emission is still dominated by the hot dust, even in the integrated spectral energy distribution.

5.3. *Infrared-to-Optical Colors of X-Ray-Selected AGNs*

In Figure 4 we show the 24-to-8 μm versus 24-to-0.7 μm color-color diagram for our sources (see Yan et al. [2004] for the location of different populations in this color-color space). The 24-to-8 μm and 24-to-0.7 μm colors are defined as $f(24:8) = \log_{10}[\nu f_\nu(24\ \mu\mathrm{m})/\nu f_\nu(8\ \mu\mathrm{m})]$ and $f(24:R) = \log[\nu f_\nu(24\ \mu\mathrm{m})/\nu f_\nu(0.7\ \mu\mathrm{m})]$, respectively. Here $f(24:R)$ is a good indicator of obscuration and/or redshift, and $f(24:8)$ has been used as a crude measure of the spectral slope and hence the dust temperature distribution and whether the source is AGN- or starburst-dominated. Brand et al. (2006b) find that AGN-dominated sources tend to have $f(24:8) < 0.3$ and starburst-dominated sources tend to have $f(24:8) > 0.3$. Even though the X-ray-selected sources must harbor a powerful AGN, their 24-to-8 μm colors suggest that the sources are dominated by a combination of AGNs and starbursts. We suggest that this diagnostic breaks down for obscured sources due to the heavy absorption at near-infrared wavelengths which will steepen the infrared slope regardless of the underlying power source. In addition, at $z \approx 1$–2, the silicate absorption feature is moving through the 24 μm filter, complicating the interpretation further.

The $R - [24]$ colors of the X-ray-selected sources are typically bluer than those of the most extreme IRS sources presented in Houck et al. (2005) and Weedman et al. (2006b), which typically have $R - [24] > 15$ [$f(24:R) > 1.83$]. The faintest optical magnitude is relatively bright ($R = 23.7$) despite the fact that there are no optical selection criteria against including optically faint sources. We suggest that the X-ray selection is biasing us against the most heavily absorbed (and therefore optically faintest) sources. Indeed, the sources in the X-ray bright subsample have among the bluest $R - [24]$ colors due at least partially to their relatively bright R-band magnitudes.

5.4. *Correlations between Infrared and X-Ray Properties*

Figure 5 shows the observed X-ray flux as a function of the X-ray hardness ratio for the combined sample of Boötes and SWIRE X-ray IRS sources. There are no sources with both small X-ray fluxes and small X-ray hardness ratios. The gray scale shows that this is not seen in the larger population of X-ray sources in the same redshift range and only becomes apparent when we jointly select X-ray sources that are both infrared bright and optically faint. Our selection criteria result in a sample of bolometrically luminous high-redshift AGNs. In these cases, small observed X-ray fluxes will be associated with more obscured sources which will also have larger hardness ratios.

For our combined sample, the absorption-dominated sources tend to have fainter X-ray fluxes and larger X-ray hardness ratios (with a median value of HR = 0.55), which are indicative of more absorbed X-ray spectra and larger H I column densities. Conversely, the power-law sources have brighter X-ray fluxes and smaller hardness ratios (with a median value of HR = −0.2), indicative of less obscured X-ray spectra and smaller H I column densities. This suggests that the dusty absorbing regions responsible for silicate absorption also contain sufficient gas to cause

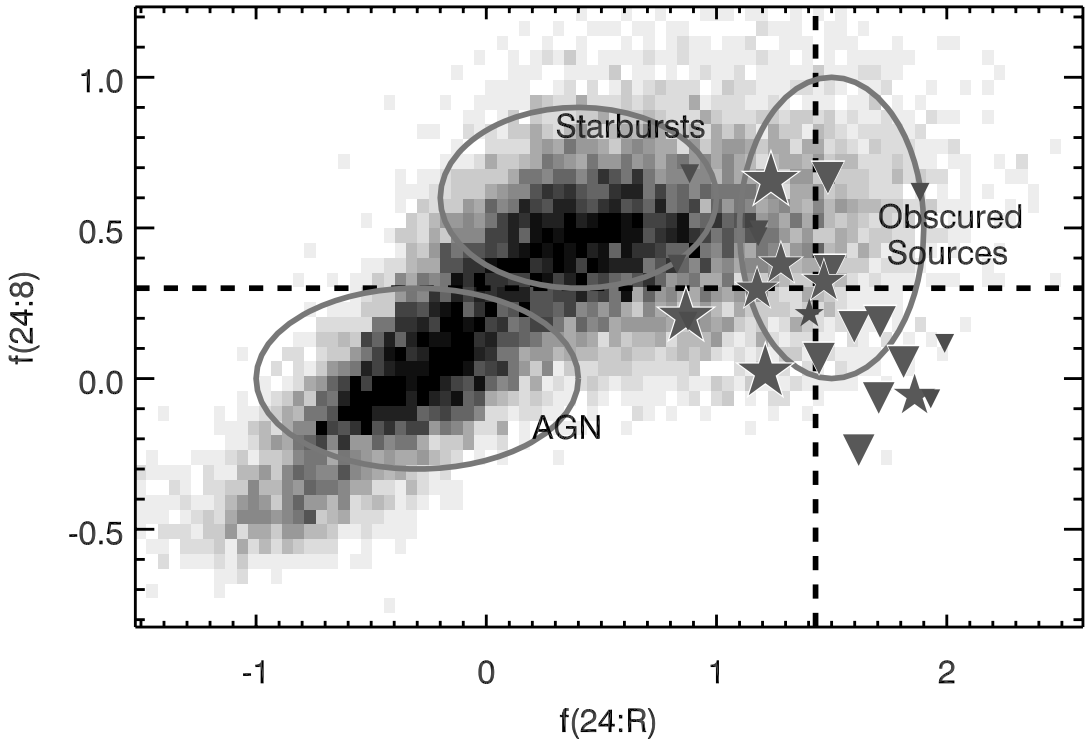

FIG. 4.—The 24-to-8 μm vs. 24-to-0.7 μm color-color diagram for X-ray-selected IRS sources. The 24-to-8 μm and 24-to-0.7 μm colors are defined as $f(24:8) = \log_{10}[\nu f_\nu(24\ \mu\mathrm{m})/\nu f_\nu(8\ \mu\mathrm{m})]$ and $f(24:R) = \log_{10}[\nu f_\nu(24\ \mu\mathrm{m})/\nu f_\nu(0.7\ \mu\mathrm{m})]$, respectively. The symbols and colors are the same as in Fig. 3. The vertical dashed line shows the $R - [24] > 14\{\log[\nu f_\nu(24)/\nu f_\nu(R) > 1.43]\}$ criteria used to select the powerful obscured sources presented in Houck et al. (2005) and Weedman et al. (2006b). The horizontal dashed line shows the 24-to-8 μm color criteria used by Brand et al. (2006b) to roughly divide steep-spectrum starburst sources from shallow-spectrum AGN-dominated sources at $z > 0.6$. [*See the electronic edition of the Journal for a color version of this figure*.]

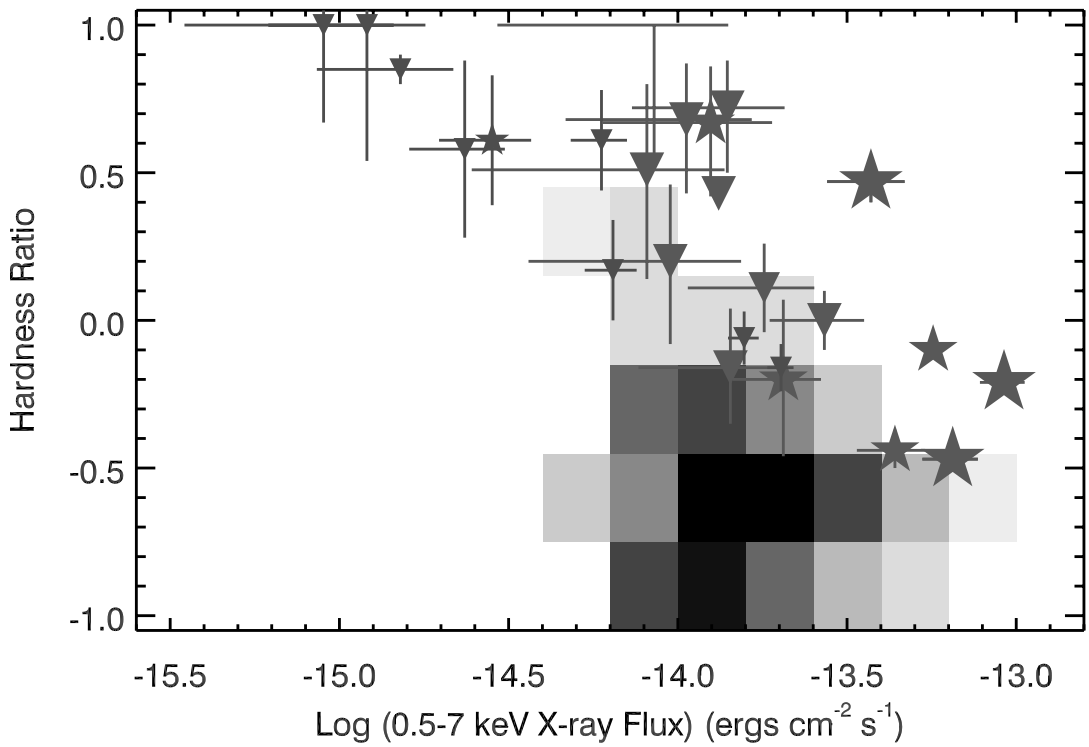

FIG. 5.—The 0.57 keV band X-ray flux vs. X-ray hardness ratio for X-ray-selected IRS sources. The hardness ratios can range from 1 (hardest X-ray spectrum) to -1 (softest X-ray spectrum). The Boötes X-ray-selected sources are denoted by large symbols (with the largest symbols denoting the X-ray bright subsample). The fainter X-ray sources from Weedman et al. (2006a) are also shown (*small symbols*). The sources are split into silicate absorption-dominated sources (*triangles*) and power-law-dominated sources (*stars*). Poisson error bars are also shown. The gray scale shows the distribution of all X-ray sources in the XBoötes survey with redshifts $z = 0.9$–2.6. [*See the electronic edition of the Journal for a color version of this figure*.]

X-ray absorption or that both the gas and dust lie along similar lines of sight. Deeper silicate absorption features may be associated with more embedded AGNs with higher column densities of gas. Our results are consistent with those of Shi et al. (2006), who measure the silicate absorption depth for a sample of 85 nearby AGNs with X-ray data and find a correlation between the strength of the silicate feature and the H I column density. Our lack of redshifts for the power-law sources means that we must compare the X-ray fluxes and hardness ratios rather than the X-ray luminosities and fitted H I column densities. Any large difference in the redshift distribution of the two populations could affect our results (e.g., higher redshift sources with identical X-ray luminosities will have softer X-ray spectra and smaller X-ray fluxes). However, in § 4.2 we argue that the power-law sources lie at $z < 2.6$, and there is no reason to think that they lie at redshifts significantly different from those of the absorption-dominated sources, given their similar selection criteria.

Although we find a trend in the X-ray and infrared properties of these sources, the correlations are only weak. The difficulty in establishing a clear relation between X-ray and infrared properties may be explained by the distribution of their gas and dust. Risaliti et al. (2002) show that the X-ray-absorbing column density of Seyfert 2 galaxies varies on yearly timescales for most sources. This suggests that most of the X-ray absorption must occur on subparsec scales. They obtain even tighter constraints in Risaliti et al. (2007) for a Seyfert galaxy which exhibits spectral variation on timescales of days. This suggests that, at least for less powerful sources, the obscuring gas is on a scale similar to that of the broad-line region. Significant amounts of dust are unlikely to lie at these distances because of the dust sublimation temperatures. The difference in the location of much of the gas and dust may explain the large scatter between parameters tracing the X-ray and mid-infrared obscuration (e.g., Rigby et al. 2004). Levenson et al. (2007) suggest that the obscuring material in dusty AGNs is likely to consist of both dense clumpy clouds of dust and a smoother intercloud medium. They argue that deep silicate absorption can only be produced in a source embedded in a smooth medium, since clumpy clouds will provide direct views of portions of illuminated clouds which will fill in the resultant silicate absorption feature. Since our X-ray-selected sources have shallower silicate absorption features than typical ULIRGs, this may suggest that they are dominated by clumpy obscuration. Alternatively, they may simply have a smaller line-of-sight obscuration.

Sturm et al. (2006) obtained IRS spectra for a sample of seven X-ray-selected AGNs which were specifically chosen to have large X-ray luminosities and large column densities of gas (due to their large X-ray hardness ratios). Given the correlation between H I column density and silicate absorption strength (see discussion above and Shi et al. 2006), we might expect them to exhibit deep silicate features. However, all of their sources exhibit featureless power-law spectra. The solution to this apparent problem may be that they selected a highly unusual population of sources which were both extremely X-ray luminous and X-ray obscured. Figure 5 shows that although X-ray obscured sources are more likely to have silicate absorption features, X-ray luminous sources are likely to have featureless power-law spectra. Perhaps more luminous AGNs are more capable of breaking up the surrounding dust into discrete clouds, which fill in the silicate absorption feature in these cases despite the large column densities of gas.

We compare the fraction of power-law-dominated to absorption-dominated sources in different samples. Weedman et al. (2006a) probe the lowest X-ray luminosities and find that only 1 out of 9 (11%) are power-law-dominated. Our sample has higher X-ray luminosities, and we find the fraction of power-law-dominated

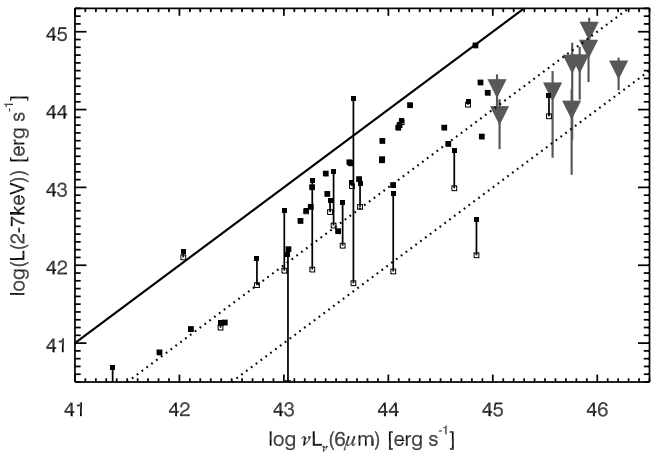

FIG. 6.—Rest-frame 6 μm luminosity against rest-frame absorption-uncorrected 2–7 keV X-ray luminosity for absorption-dominated Boötes sources (*triangles*). The Poisson error bars are shown for the X-ray luminosity. The low-redshift *ISO* sources from Lutz et al. (2004) are plotted as squares (connected open and filled squares denote X-ray luminosities uncorrected and corrected for X-ray absorption, respectively). The solid line shows a direct correspondence between the X-ray and 6 μm luminosities. The dotted lines show where $L(2\text{–}7\ \text{keV}) = 0.1\nu L_\nu(6\ \mu\text{m})$ and $L(2\text{–}7\ \text{keV}) = 0.01\nu L_\nu(6\ \mu\text{m})$. [*See the electronic edition of the Journal for a color version of this figure.*]

to absorption-dominated sources to be 4 out of 13 (31%) in the main sample and 7 out of 16 (43%) in the total (main + X-ray bright) sample. All of the sources in the Sturm et al. (2006) study are power-law-dominated. Their sources are particularly bright in the X-ray, with intrinsic X-ray luminosities in the range $\log L_X = 44.0\text{–}45.5$. This suggests that more X-ray luminous sources are more likely to have shallower silicate absorption (which will appear as power-law sources).

Krabbe et al. (2001), Lutz et al. (2004), and Horst et al. (2006) show that there is a strong relation between AGN hard X-ray emission and mid-infrared continuum in low-redshift active galaxies. Figure 6 shows the AGN continuum luminosity at 6 μm as a function of 2–7 keV X-ray luminosity for the absorption-dominated sources (the power-law sources could not be included because we do not have redshifts to derive the luminosities). Although the absorption-dominated sources do not show a clear correlation between these two quantities, this lack is likely to be due to the large luminosity errors and relatively narrow luminosity range of the sample. When we compare our sources with lower luminosity sources at low redshift (Lutz et al. 2004), we find that they form the higher luminosity extension of the relation. We have chosen not to correct the X-ray luminosity for absorption, given the large uncertainties. Seven out of 9 of our sources lie at $L(2\text{–}7\ \text{keV})/\nu L_\nu(6\ \mu\text{m}) < 0.1$, compared to only 8 out of 47 of the Lutz et al. (2004) sources (before correcting for absorption). This suggests that our sources are generally more obscured than the low-redshift, lower luminosity AGNs presented in Lutz et al. (2004).

6. CONCLUSIONS

We have presented mid-infrared spectra obtained using the *Spitzer* IRS of a sample of 16 X-ray loud 24 μm sources. The spectra of these sources are characterized by either silicate absorption or a featureless power law, with no evidence of PAH emission. This suggests that the mid-infrared emission from these sources is dominated by warm dust emission surrounding the active nucleus with little contribution from star formation. The absorption-dominated sources lie in the range $0.9 < z < 2.6$ and have very

high X-ray and infrared luminosities ($\log L_{\rm IR} = 12.5$–$13.6\ L_{\odot}$). The average absorption depth in our absorption-dominated X-ray sources is similar to that of local Seyfert 2 AGNs and much smaller than that of typical ULIRGs. This suggests a difference in the distribution of the dusty material between our sample and typical ULIRGs. The weak silicate absorption feature in our sample could indicate a more clumpy dust distribution or a lower line-of-sight obscuration. There is evidence in the average spectrum for weak [Ne II], [Ne V], and [Ne III] lines. The [Ne V] is relatively stronger than is seen in local Seyferts, suggesting a higher ionization of the narrow-line region in these more powerful AGNs. Given their higher X-ray fluxes, it is unlikely that the power-law sources lie at $z > 2.6$. Instead, they must have only weak silicate absorption or emission features. Comparison with other samples suggests that the fraction of power-law sources appears to increase with X-ray luminosity and decrease with X-ray obscuration. Both the infrared and infrared-to-optical colors suggest that the sources are relatively unobscured compared with $R - [24] > 15$ sources. Our X-ray selection is likely to be preferentially biased to less obscured and/or more powerful AGNs. We find that sources with silicate absorption features tend to have fainter X-ray fluxes and larger hardness ratios. This suggests that more absorbed sources also have higher column densities of absorbing gas along the same line of sight.

We thank our colleagues on the NDWFS, XBoötes, MIPS, IRS, AGES, and IRAC teams. K. B. is supported by the Giacconi Fellowship at STScI. This research is supported by the National Optical Astronomy Observatory, which is operated by the Association of Universities for Research in Astronomy, Inc., under a cooperative agreement with the National Science Foundation. Support for this work by the IRS GTO team at Cornell University was provided by NASA through contract No. 1257184 issued by JPL/Caltech. This work is based on observations made with the *Spitzer Space Telescope*, which is operated by the Jet Propulsion Laboratory, California Institute of Technology, under a contract with NASA. The *Spitzer* MIPS survey of the Boötes region was obtained using GTO time provided by the *Spitzer* Infrared Spectrograph Team (PI: J. Houck) and M. Rieke. The IRS was a collaborative venture between Cornell University and Ball Aerospace Corporation funded by NASA through the Jet Propulsion Laboratory and the Ames Research Center. We thank the anonymous referee for useful comments.

REFERENCES

Armus, L., et al. 2007, ApJ, 656, 148
Brand, K., et al. 2006a, ApJ, 641, 140
———. 2006b, ApJ, 644, 143
———. 2007, ApJ, 663, 204
———. 2008, ApJ, 673, 119
Brandl, B. R., et al. 2006, ApJ, 653, 1129
Brown, M. J. I., et al. 2006, ApJ, 638, 88
Caputi, K. I., et al. 2007, ApJ, 660, 97
Desai, V., et al. 2007, ApJ, 669, 810
Dey, A., et al. 2008, ApJ, 677, 943
Draine, B. T. 2003, ApJ, 598, 1017
Eisenhardt, et al. 2004, ApJS, 154, 48
Elston, R. J., et al. 2006, ApJ, 639, 816
Farrah, D., et al. 2007, ApJ, 667, 149
Fiore, F., et al. 2008, ApJ, 672, 94
Genzel, R., et al. 1998, ApJ, 498, 579
Grimm, H.-J., Gilfanov, M., & Sunyaev, R. 2003, MNRAS, 339, 793
Hao, L., Weedman, D. W., Spoon, H. W. W., Marshall, J. A., Levenson, N. A., Elitzur, M., & Houck, J. R. 2007, ApJ, 655, L77
Hickox, R. C., et al. 2007, ApJ, 671, 1365
Higdon, S. J. U., et al. 2004, PASP, 116, 975
Horst, H., Smette, A., Gandhi, P., & Duschl, W. J. 2006, A&A, 457, L17
Houck, J. R., et al. 2004, ApJS, 154, 18
———. 2005, ApJ, 622, L105
Jannuzi, B. T., & Dey, A. 1999, in ASP Conf. Ser. 191, Photometric Redshifts and the Detection of High Redshift Galaxies, ed. R. Weymann et al. (San Francisco: ASP), 111
Kenter, A., et al. 2005, ApJS, 161, 9
Krabbe, A., Böker, T., & Maiolino, R. 2001, ApJ, 557, 626
Lacy, M., et al. 2004, ApJS, 154, 166
Levenson, N. A., Sirocky, M. M., Hao, L., Spoon, H. W. W., Marshall, J. A., Elitzur, M., & Houck, J. R. 2007, ApJ, 654, L45
Lonsdale, C., et al. 2004, ApJS, 154, 54
Lutz, D., Maiolino, R., Spoon, H. W. W., & Moorwood, A. F. M. 2004, A&A, 418, 465
Lutz, D., Spoon, H. W. W., Rigopoulou, D., Moorwood, A. F. M., & Genzel, R. 1998, ApJ, 505, L103
Murray, S. S., et al. 2005, ApJS, 161, 1
Pope, A., et al. 2008, ApJ, 675, 1171
Rieke, G. H., et al. 2004, ApJS, 154, 25
Rigby, J. R., et al. 2004, ApJS, 154, 160
Rigopoulou, D., Spoon, H. W. W., Genzel, R., Lutz, D., Moorwood, A. F. M., & Tran, Q. D. 1999, AJ, 118, 2625
Risaliti, G., Elvis, M., Fabbiano, G., Baldi, A., Zezas, A., & Salvati, M. 2007, ApJ, 659, L111
Risaliti, G., Elvis, M., & Nicastro, F. 2002, ApJ, 571, 234
Sajina, A., Yan, L., Armus, L., Choi, P., Fadda, D., Helou, G., & Spoon, H. 2007, ApJ, 664, 713
Sanders, D. B., Soifer, B. T., Elias, J. H., Madore, B. F., Matthews, K., Neugebauer, G., & Scoville, N. Z. 1988, ApJ, 325, 74
Shi, Y., et al. 2006, ApJ, 653, 127
Spoon, H. W. W., Marshall, J. A., Houck, J. R., Elitzur, M., Hao, L., Armus, L., Brandl, B. R., & Charmandaris, V. 2007, ApJ, 654, L49
Stark, A. A., Gammie, C. F., Wilson, R. W., Bally, J., Linke, R. A., Heiles, C., & Hurwitz, M. 1992, ApJS, 79, 77
Stern, D., et al. 2005, ApJ, 631, 163
Sturm, E., Hasinger, G., Lehmann, I., Mainieri, V., Genzel, R., Lehnert, M. D., Lutz, D., & Tacconi, L. J. 2006, ApJ, 642, 81
Tran, Q. D., et al. 2001, ApJ, 552, 527
Weedman, D. W., et al. 2005, ApJ, 633, 706
———. 2006a, ApJ, 653, 101
———. 2006b, ApJ, 651, 101
Yan, L., et al. 2004, ApJS, 154, 60
———. 2007, ApJ, 658, 778